



RESEARCH PAPER

 OPEN ACCESS 

## Genomic map of candidate human imprint control regions: the imprintome

Dereje D. Jima<sup>a,b</sup>, David A. Skaar<sup>a,c,d</sup>, Antonio Planchart<sup>a,c,d</sup>, Alison Motsinger-Reif<sup>b,c,e</sup>, Sebnem E. Cevik<sup>d</sup>, Sarah S. Park<sup>d,f</sup>, Michael Cowley <sup>a,c,d</sup>, Fred Wright<sup>a,b</sup>, John House<sup>b,c,d,e</sup>, Andy Liu<sup>g</sup>, Randy L. Jirtle <sup>a,c,d</sup>, and Cathrine Hoyo<sup>a,c,d</sup>

<sup>a</sup>Center for Human Health and the Environment, North Carolina State University, Raleigh, NC, USA; <sup>b</sup>Bioinformatics Research Center, North Carolina State University, Raleigh, NC, USA; <sup>c</sup>Department of Biological Sciences, North Carolina State University, Raleigh, NC, USA; <sup>d</sup>Toxicology Program, North Carolina State University, Raleigh, NC, USA; <sup>e</sup>National Institute of Environmental Health Sciences, Research Triangle Park, NC, USA; <sup>f</sup>Environmental Protection Agency, Research Triangle Park, NC, USA; <sup>g</sup>Department of Neurology, Duke University, School of Medicine, Durham, NC, USA

### ABSTRACT

Imprinted genes – critical for growth, metabolism, and neuronal function – are expressed from one parental allele. Parent-of-origin-dependent CpG methylation regulates this expression at imprint control regions (ICRs). Since ICRs are established before tissue specification, these methylation marks are similar across cell types. Thus, they are attractive for investigating the developmental origins of adult diseases using accessible tissues, but remain unknown. We determined genome-wide candidate ICRs in humans by performing whole-genome bisulphite sequencing (WGBS) of DNA derived from the three germ layers and from gametes. We identified 1,488 hemi-methylated candidate ICRs, including 19 of 25 previously characterized ICRs (<https://humanicr.org/>). Gamete methylation approached 0% or 100% in 332 ICRs (178 paternally and 154 maternally methylated), supporting parent-of-origin-specific methylation, and 65% were in well-described CTCF-binding or DNaseI hypersensitive regions. This draft of the human imprintome will allow for the systematic determination of the role of early-acquired imprinting dysregulation in the pathogenesis of human diseases and developmental and behavioural disorders.

### ARTICLE HISTORY

Received 16 April 2022  
Accepted 15 June 2022

### KEYWORDS

Epigenetics; genomic imprinting; foetal origins; whole genome; methylation; imprint control regions

## Introduction


Data from model systems and humans demonstrate that environmentally induced epigenetic modifications occurring early in development can cause long-term gene expression changes in important mechanistic pathways involved in disease pathogenesis. Affected diseases include neurological disorders [1,2], cardio- and cerebrovascular diseases [3], and cancers [4–6], and their major risk factors, such as obesity and the attendant dysfunction in metabolism, nutrient acquisition, fat deposition, appetite, and satiety [7,8].

Covalent DNA methylation of cytosines in CpG dinucleotide sites is the most studied epigenetic modification and is hypothesized to link environmental exposures to these diseases. Nevertheless, data generated from case-control or cross-sectional studies, the most cost-efficient epidemiologic study designs, have been difficult to interpret.

This is because methylation marks measured in easily accessible peripheral cell types from otherwise healthy individuals do not always reflect methylation in inaccessible cell types, tissues, and organs involved in the formation or progression of a chronic disease. Moreover, DNA methylation at susceptible loci can adaptively change throughout life in response to environmental exposures or disease. Indeed, methylation levels can also naturally diverge with normal cell differentiation, ageing, and environmental influences [9–12].

Known exceptions are CpG methylation marks that are stochastically established before specification that control metastable epiallele expression [13] and imprinting control regions (ICRs) that regulate the monoallelic expression of imprinted genes [6,14]. CpG methylation of metastable epialleles and ICRs is established before gastrulation and is mitotically heritable. Thus, these epigenetic

**CONTACT** Cathrine Hoyo  [choyo@ncsu.edu](mailto:choyo@ncsu.edu); Randy L. Jirtle  [rljirtle@ncsu.edu](mailto:rljirtle@ncsu.edu)  Department of Biological Sciences, North Carolina State University, Raleigh, NC, USA

 Supplemental data for this article can be accessed online at <https://doi.org/10.1080/15592294.2022.2091815>

© 2022 The Author(s). Published by Informa UK Limited, trading as Taylor & Francis Group.  
This is an Open Access article distributed under the terms of the Creative Commons Attribution-NonCommercial-NoDerivatives License (<http://creativecommons.org/licenses/by-nc-nd/4.0/>), which permits non-commercial re-use, distribution, and reproduction in any medium, provided the original work is properly cited, and is not altered, transformed, or built upon in any way.

marks are normally similar across tissues and cell types throughout an individual's life. Unlike metastable epialleles however, ICRs are defined by parent-of-origin specific methylation marks that are important gene dosage regulators based on the allele's parental origin. Consequently, in contrast to epigenetic marks controlling metastable epiallele expression, methylation marks regulating imprinted genes are similar across individuals [15,16]. Importantly, changes in the methylation patterns in ICRs are implicated in adult-onset diseases suspected to have foetal origins, including neurological disorders, cancers, and metabolic diseases stemming from abnormal growth and nutrient acquisition disorders [17,18].

Together, these features make ICRs attractive targets for dissecting disease aetiology, particularly since imprinted genes comprise an estimated 1–6% of the human genome, are over-selected for growth regulators, and are critical in early embryonic development [3,19]. The stability of these methylation marks with age also makes them long-term 'records' of early exposures that are difficult to obtain through questionnaires or other exposure assessment assays [6]. Yet, despite their biological and clinical relevance, only 25 of the ICRs regulating the 100–150 identified human imprinted genes, and of the 300–1,000 genes predicted to be imprinted [19], are currently known [14].

Leveraging existing specimens, recent advances in genome sequencing, and computational capabilities, we sought to comprehensively characterize human ICRs using DNA methyl-sequencing of tissues representing the three germ layers as well as the gametes, to create a catalogue of the set of imprint regulatory DNA methylation marks in humans, the 'human imprintome' [14]. This characterization of human ICRs should enable a more detailed understanding of the epigenetic basis of numerous pathophysiologies with foetal origins, and with that, advance the ability to diagnose, prevent, and treat a number of developmental disorders and diseases.

## Materials and methods

### Materials and subjects

Sperm from three adults and tissues from twelve 65 to 95-day-old embryos of both sexes (confirmed by sex-linked marker genotyping) and of African and European descent were selected for bisulphite DNA sequencing. These tissues were obtained from the National Institutes of Health funded Laboratory of Human Embryology at the University of Washington, Seattle, WA; they were snap frozen to preserve DNA/RNA integrity (NCSU Institutional Review Board #3565). Embryonic tissues were used for identifying ICRs because the gametic and somatic imprint marks are intact, and because monoallelic gene expression of imprinted genes occurs primarily during embryonic development [20–23]. Sperm DNA was from the TIEGER study at Duke [23].

### Whole-genome bisulphite sequencing (WGBS)

Libraries for NextSeq sequencing using HiSeq 2500 were prepared from bisulphite converted DNA derived from tissues representing the three germ layers using previously described methods [21]. Thirty (three from sperm obtained as previously described [23,24] and 27 from somatic tissues) of the 36 samples passed quality control standards for sequencing by Illumina NextSeq with 12–15X coverage. The sequenced somatic tissue libraries were 8 kidney (mesoderm), 8 liver (endoderm), and 11 brain (ectoderm). Libraries were index-tagged for separating reads after multiplex sequencing and pooled into groups of nine, with each group split for sequencing into three separate lanes. Splitting samples across lanes ensured that no single sample was disproportionately affected by technical variability specific to an individual sequencing lane (e.g., low read numbers or low read quality). If a problem persisted, samples exhibiting consistently low quality across lanes were rerun or removed from analysis. These sequence data were supplemented with publicly available oocyte sequence data (JGAS0000000006) [25] and part of control sperm data from PRJNA754049 (control males in

this study were otherwise healthy individuals who did not use cannabis) [26]. Details are in the Supplementary Materials and Methods.

### **Bioinformatic approaches to identify ICRs**

Samples were separated by index sequences and aligned to a reference *in silico* bisulphite-converted genome. Reads without unique alignment to the reference sequence due to either repetitive sequence or loss of information because of cytosine conversion were eliminated, as were duplicate reads, indicative of clonally amplified original random DNA fragments. From these reads, methylation fractions and read counts were calculated for all CpG sites in the genome. We developed a candidate ICR identification pipeline (putICR) application using a Ruffus framework in Python. The workflow is described in detail in Supplementary Materials and Methods and outlined in Supplementary Figure S7.

This application was designed to scan the genome and identify regions of allelic differential methylation based on four criteria that define genomic imprinting: 1)  $\geq 5$  consecutive CpG sites, consistent with known cis-acting imprinted control regions [14]; 2) methylation levels of  $50\% \pm 15\%$ , supportive of monoallelic methylation (i.e., approximately 100% methylation on one parental allele and 0% on the other); 3) similarity of methylation levels in tissues from the three germ layers (i.e., brain, liver, and kidney), as expected for methylation marks established before tissue specification; and 4) similarity of methylation across individuals, indicative of sequence regions playing critical roles in regulating imprinted gene dosage, which should not generally vary by sex, ethnicity, developmental age, or from person-to-person. Based on the methylation levels, we developed an online tool, the imprintome browser, which is linked to standard genome browsers to visualize the methylation level for each CG site in the 1,488 candidate ICR regions (<https://humanicr.org/>).

To assess the reproducibility of the putICR pipeline, the raw sequence data and the same four criteria were provided to an independent bioinformatics group (Sciome, Inc, Research Triangle Park, NC) (Supplementary Materials and Methods). Additionally, fully methylated or unmethylated regions from gametic sequences

were compared, as these are the original inherited parent-of-origin specific regions.

We used pyrosequencing (sequencing primers in Supplementary Table S3) to determine if methylation patterns at previously identified ICRs in the three germ layers in embryos were similar to those obtained from DNA from accessible adult tissues frequently used in epidemiologic studies, such as peripheral blood components and human umbilical vein endothelial cells (HUVECs) (Figure 3).

## **Results**

### **WGBS library preparation**

WGBS libraries were prepared from three human tissues – brain (ectoderm), kidney (mesoderm), and liver (endoderm) – representing the three germ layers from 12 embryos (6 male, 6 female), and three sperm samples, resulting in 39 total libraries. Twenty-seven of the tissue libraries (i.e., 8 kidney (mesoderm), 8 liver (endoderm), and 11 brain (ectoderm)), and the three sperm libraries passed quality checks for Illumina HiSeq2500 (Illumina, San Diego, California, USA), resulting in 30 total libraries sequenced (27 somatic and 3 gametic). Gametic sequence data were augmented with publicly available human oocyte sequence data (accession number JGAS0000000006 [25]) and control sperm sequence data from PRJNA754049 [26]. The average number of per-sample reads was 153 million (range 74–231 million), covering an average of 23.1 billion bases per sample (range 11.2–34.9 billion). Approximately 80% of reads uniquely aligned to the *in silico* bisulphite-converted human genome (hg38). Of the 29.2 million CpG sites in the human genome [27], an average of 26.6 million (91%, range 86–94%) were covered by aligned reads for the set of 30 samples.

### **Characteristics of candidate ICRs from tissues representing the three germ layers**

Most of the sequences obtained from the brain, kidney, and liver (75%) had a sequence coverage of greater than 20X. The sequence coverage for oocytes (accession number JGAS0000000006) was lower due to the decreased availability of DNA from this source [25] while the sperm coverage, by incorporating data

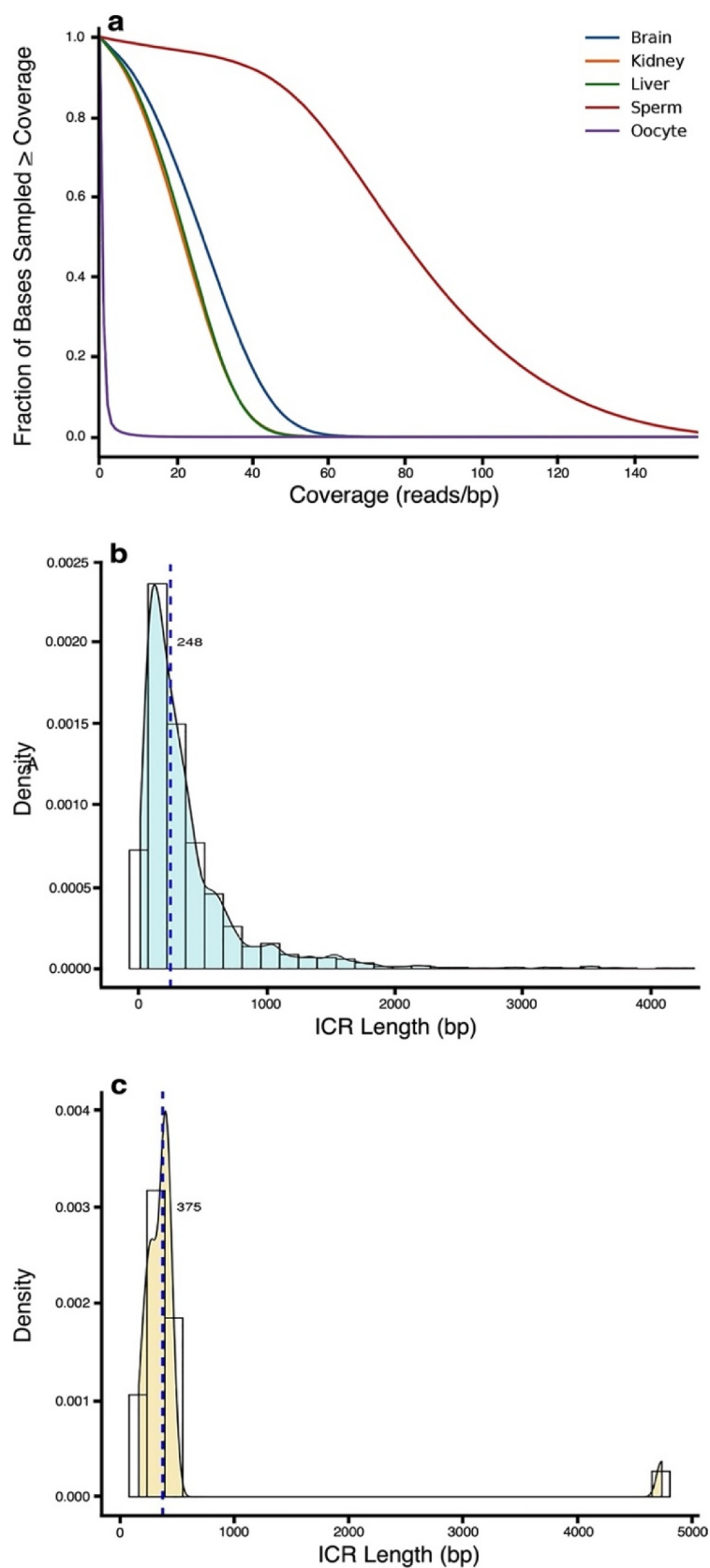


**Figure 1.** Detection of ICRs genome-wide. A bioinformatics selection algorithm, putICR, was used to identify methylation fractions using whole-genome bisulphite sequencing (WGBS) of DNA from kidney, liver, and brain embryonic tissues and gametes (i.e., sperm and oocyte). (a) Genome coverage was  $>20\times$  for the somatic tissues in more than 75% of the fraction base sampled. The genome coverage was lower in the available oocyte gametic sequence data (accession number JGAS0000000006), but higher in sperm because our data were supplemented with control sperm data from PRJNA754049 [25,26]. (b) The size range of candidate imprint control regions (ICRs) averaged 248 bp. (c) This is similar to previously identified ICRs (Avg: 375 bp) [14].



from Schrott et al. [26], was higher (Figure 1 (a)). Using the percent methylation fractions calculated for each CpG site, candidate ICRs were defined based on the following criteria: five or more consecutive CpG sites within a 300 bp region having methylation levels of approximately  $50 \pm 10$ –20% in tissues from all three germ layers. These criteria are consistent with an ICR being a genomic series of cis-acting CpG sites that are established in embryonic stem cells, resulting in one parental allele being near fully methylated (~100%) while the other is unmethylated (~0%) for  $\geq 80\%$  of the sites.

Using the most relaxed criteria ( $50 \pm 20\%$ ), we identified 7,559 candidate ICRs, including 21 of the 25 known ICRs [14]. A more stringent methylation criterion of  $50 \pm 15\%$  decreased the number of candidate ICRs to 1,488 while still detecting 19 of 25 known ICRs (Table 1 and Supplementary Table S1). Further, restricting the window to  $50\% \pm 10\%$  decreased the number of candidate ICRs to 127, including 15 of the known ICRs.

The 1,488 novel ICRs methylated at  $50\% \pm 15\%$  ranged from 10 to ~4,000 bp long, with a median length of 248 bp (Figure 1(b)). This is similar to the median size of the known ICRs (375 bp) (Figure 1(c)), but with a tailing distribution of much longer candidates. As expected for ICRs, differentiated tissues derived from the three embryonic germ layers exhibited similar methylation levels, consistent with the establishment of these methylation marks in the stem cells before tissue specification. Importantly, these regions also showed similar methylation fractions across individuals, consistent with ICRs controlling gene dosage. We have developed a corresponding imprintome browser depicting methylation fractions for each CpG site in the 1,488 candidate ICRs identified for each embryonic germ layer (<https://humanicr.org/>).

As a sensitivity analysis, Sciome, Inc. (Research Triangle Park, NC, USA) used an independent calling pipeline with similar procedures for adapter trimming and alignment to hg38 and the four ICR call criteria, but without pooling aligned reads. This generated 1,225 ICRs, including 19 of the 25 characterized ICRs. Of the 1,225 ICRs discovered by Sciome, Inc. (Research Triangle Park, NC, USA), 900 (62%) were found in our initial

analysis (Supplementary Table S1 and Supplementary Table S2).

### Parent-of-origin methylation patterns in gametes

Parent-of-origin methylation patterns are a property of authentic inherited ICRs and can be discerned from the methylation patterns of gametes. We examined the parent-of-origin methylation patterns of the novel ICRs using WGBS results from sperm and oocyte sequence data. Oocyte data was obtained from public databases (accession number JGAS00000000006) [25]. Our sperm sequence data was supplemented with partial control sperm samples from PRJNA754049 [26]. We compared the embryonic and gametic methylation patterns of the 1,488 candidate ICRs seeking to identify those either fully unmethylated (<10%) or fully methylated (>90%) in gametes. This methylation pattern indicates control of genomic imprinting, which once established in the gametes and inherited persists throughout development. As proof of concept, we first examined whether this strategy could successfully identify known ICRs, and 19 of the 25 known ICRs [14] were captured using this strategy (Table 1 and Supplementary Table S1). Despite the low read-depth of the oocyte sequence data, we found that 332 (Table 1) of the 1,488 candidate ICRs (Supplementary Table 1) had methylation patterns consistent with originating in either the sperm or egg (visualize in <https://humanicr.org/>).

Our data show that two previously characterized ICRs [14], *PLAGL1* (ICR\_404, Figure 2(a), Table 1 and Supplementary Table S1) and *MEG3* (ICR\_872, 873, Figure 2(b), Table 1 and Supplementary Table S1) have somatic DNA methylation approximating the expected 50% level, but they appear significantly longer than the regions currently defined for these ICRs. Additional examples of this are shown for imprinted genes *L3MBTL1* (ICR\_1194, Supplementary Figure S1A, Table 1 and Supplementary Table S1) [28] and *BLCAP/NNAT* (ICR\_1192, 1193, Supplementary Figure S1B, Table 1 and Supplementary Table S1) [29,30].

The ICRs for most known imprinted human genes (<https://www.geneimprint.com/site/genes-by-species>) are unknown, but most are now

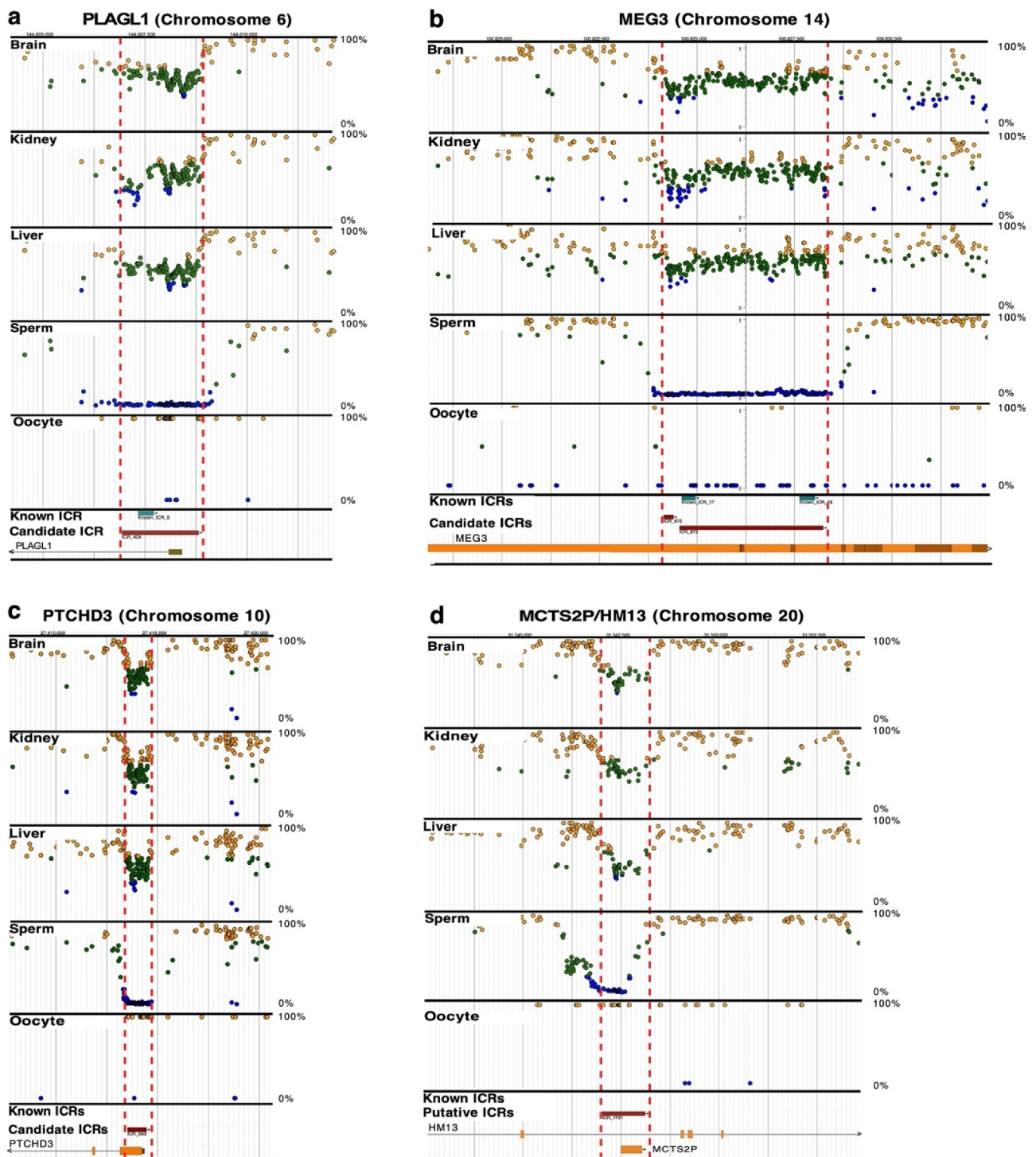


**Figure 2.** Previously known and candidate ICRs. (a) *PLAGL1* (ICR\_404) and (b) *MEG3* (ICR\_872,873) imprinted genes contain previously known ICRs (blue boxes) [14]. They were also identified in our whole-genome bisulphite sequencing (WGBS) screen for candidate ICRs (red boxes); visualize at <https://humanicr.org/>. The ICRs defined herein overlap and extend beyond the currently known ICRs. (c) *PTCHD3* (ICR\_643) and (d) *MCTS2P/HM13* (ICR\_1191) contain only candidate ICRs (red boxes) determined in this study, and potentially control novel imprinted genes. The methylation levels for ICRs is  $50 \pm 15\%$  for the candidate ICRs. DNA methylation levels determined by WGBS in sperm and oocytes are also provided. These sequence data were supplemented with publicly available gametic sequence (accession number JGAS0000000006) and part of the control sperm data from PRJNA754049 [25,26]. Dots indicate hemi-methylation (green), hypomethylation (blue), and hypermethylation (yellow) based on WGBS. The vertical dashed red lines delineate the candidate ICR regions.

**Table 1.** Candidate ICRs<sup>+</sup> with gametic origin of methylation.

ID	Genomic Coordinates	Parental Origin of Methylation	Nearest Transcript	Distance to Nearest Transcript
ICR_2 <sup>^</sup>	chr1:628959-630792	P	MTND1P23 MTND2P28	0
ICR_3 <sup>^</sup>	chr1:632183-632834	P	MTCO1P12 MIR12136 MTCO2P12	0
ICR_4 <sup>^</sup>	chr1:633381-634921	P	MTCO2P12 MTATP8P1 MTATP6P1  MTCO3P12	0
ICR_6*	chr1:1174554-1174597	P	TLL10	0
ICR_10 <sup>^</sup>	chr1:2469095-2469433	P	PLCH2	0
ICR_12	chr1:2661644-2661722	M	TTC34	0
ICR_15	chr1:6461637-6461737	M	TNFRSF25	0
ICR_16 <sup>^</sup>	chr1:7199286-7199687	M	CAMTA1	0
ICR_17 <sup>^</sup>	chr1:8117511-8117827	P	RPL7AP18	59,024
ICR_20 <sup>^</sup>	chr1:10682902-10683413	P	CASZ1	0
ICR_21	chr1:10808891-10809149	P	CASZ1	12,241
ICR_22 <sup>^</sup>	chr1:16164023-16164515	P	EPHA2	7919
ICR_25 <sup>^</sup>	chr1:22428873-22429209	M	ZBTB40	0
ICR_26	chr1:24210504-24210603	P	LINC02800	0
ICR_32* <sup>^</sup>	chr1:32471040-32471395	M	ZBTB8B	0
ICR_35 <sup>^</sup>	chr1:35699589-35699951	M	C1orf216	13,925
ICR_36 <sup>^</sup>	chr1:36572484-36573080	P	FTLP18	57,255
ICR_39	chr1:38210131-38210429	P	LINC01343	0
ICR_40 <sup>^</sup>	chr1:39559036-39559674	M	PPIEL	0
ICR_41* <sup>^</sup>	chr1:41423557-41423666	P	FOXO6	39,967
ICR_43 <sup>^</sup>	chr1:47963613-47963993	P	TRABD2B	0
ICR_44 <sup>^</sup>	chr1:53145868-53146595	P	SLC1A7	3230
ICR_46* <sup>^</sup>	chr1:68046822-68047535	M	DIRAS3	0
ICR_47 <sup>^</sup> #	chr1:68049858-68051097	M	DIRAS3	0
ICR_48* <sup>^</sup>	chr1:68051239-68051861	M	DIRAS3	0
ICR_52 <sup>^</sup>	chr1:91171791-91172929	P	HFM1	87,837
ICR_62	chr1:148011459- 148011977	P	PDZK1P1 LINC02804	0
ICR_65	chr1:156840564- 156840978	P	NTRK1 INSRR	0
ICR_73	chr1:168056307- 168056468	M	DCAF6 GCSHP5	0
ICR_80* <sup>^</sup>	chr1:204829545- 204831249	P	NFASC	0
ICR_81 <sup>^</sup>	chr1:208044765- 208045294	P	PLXNA2	0
ICR_83 <sup>^</sup>	chr1:226127234- 226127411	P	ACBD3	17,268
ICR_100 <sup>^</sup>	chr1:234955629- 234956306	P	RN7SL668P	51141
ICR_101 <sup>^</sup>	chr1:236120016- 236120293	P	GPR137B	22236
ICR_107	chr1:245688553- 245688677	M	KIF26B	0
ICR_116 <sup>^</sup>	chr2:28342638-28342806	P	BABAM2	3737
ICR_117	chr2:31581451-31581676	M	SRD5A2	0
ICR_121 <sup>^</sup>	chr2:44885640-44886022	P	LINC01833	35,058
ICR_123 <sup>^</sup>	chr2:49229257-49229842	P	FSHR	74730
ICR_125	chr2:54289850-54290281	M	ACYP2	0
ICR_133 <sup>^</sup>	chr2:95078802-95079392	P	MRP55	5977
ICR_144	chr2:120526146- 120526533	P	LINC01101	59,797

(Continued)

Table 1. (Continued).

ID	Genomic Coordinates	Parental Origin of Methylation	Nearest Transcript	Distance to Nearest Transcript
ICR_158	chr2:161340716-161341095	M	PSMD14 MXRA7P1	0
ICR_159^	chr2:162243085-162244421	P	FAP	0
ICR_161^	chr2:173217299-173217391	M	MAP3K20	0
ICR_167^	chr2:206257411-206257639	P	HMG1P6	1989
ICR_168	chr2:206257801-206258345	P	HMG1P6	1283
ICR_169*	chr2:206258596-206260336	P	HMG1P6 RN7SKP260	0
ICR_170*	chr2:206260650-206261209	P	RN7SKP260	436
ICR_177	chr2:218890039-218890255	P	WNT10A	0
ICR_182^	chr2:234168141-234168738	P	SPP2	91,007
ICR_184*^	chr2:236642778-236643076	P	ACKR3	60,420
ICR_187*^	chr2:241901656-241902337	M	LINC01237	0
ICR_188	chr2:241902453-241902725	M	LINC01237	0
ICR_191	chr3:147595-148344	P	CHL1	48,244
ICR_194^	chr3:14366359-14366571	P	LINC01267	13,791
ICR_198	chr3:28200466-28200710	M	CMC1	40,883
ICR_199	chr3:30893926-30894319	M	GADL1	0
ICR_202	chr3:44580918-44580941	P	ZKSCAN7 MPRIIP1	0
ICR_207	chr3:50481168-50481455	P	CACNA2D2	0
ICR_209	chr3:72928978-72929098	M	GXYLT2 FTH1P23	0
ICR_227*^	chr3:147297676-147298367	P	RPL21P71	20,389
ICR_228*^	chr3:150865529-150865545	M	MINDY4B	4831
ICR_229^	chr3:156120781-156120929	M	KCNAB1	0
ICR_230^	chr3:184563668-184564356	P	EPHB3	0
ICR_239	chr4:1053635-1054116	P	RNF212	2132
ICR_243*^	chr4:2463493-2463856	M	CFAP99	530
ICR_244	chr4:3702565-3703061	P	LINC02171	24,710
ICR_246^	chr4:3771074-3771481	P	ADRA2C	2548
ICR_249	chr4:4863227-4864029	M	MSX1	0
ICR_250^	chr4:6105593-6105924	M	JAKMIP1	0
ICR_251	chr4:8581258-8581331	M	GPR78	0
ICR_254^	chr4:39406796-39407320	P	KLB	0
ICR_255	chr4:41876102-41876861	P	LINC00682	2660
ICR_263	chr4:49270757-49270848	M	MTND3P22	23,842
ICR_274	chr4:82758740-82759068	P	SCD5	0
ICR_275^	chr4:88697244-88698085	M	HERC3 NAP1L5	0
ICR_278	chr4:121932565-121932847	M	TRPC3	0
ICR_281	chr4:152009424-152009915	P	RNA5SP169	37,811

(Continued)



**Table 1.** (Continued).

ID	Genomic Coordinates	Parental Origin of Methylation	Nearest Transcript	Distance to Nearest Transcript
ICR_282	chr4:154781727-154782004	M	RBM46	0
ICR_284 <sup>^</sup>	chr4:173608770-173608942	P	MORF4	6794
ICR_295	chr4:190089486-190089578	M	DUX4L3	497
ICR_297 <sup>^</sup>	chr5:346459-346789	M	AHRR	0
ICR_300	chr5:580390-580767	P	CEP72	31,573
ICR_319 <sup>^</sup>	chr5:80650716-80650931	P	DHFR MTRNR2L2	0
ICR_323	chr5:101783627-101784015	M	OR7H2P	31868
ICR_324	chr5:110894251-110894443	M	BCLAF1P1	51,830
ICR_325 <sup>^</sup>	chr5:134927018-134927085	P	PCBD2 MTND4P12	0
ICR_326* <sup>^</sup>	chr5:136079156-136079563	M	TGFBI	15338
ICR_332	chr5:140829825-140830061	M	PCDHA1-6	0
ICR_340	chr5:141345713-141345776	M	PCDHGA1-3	0
ICR_349	chr5:158737352-158737526	M	EBF1	0
ICR_352	chr5:171319025-171319892	P	TLX3	6886
ICR_353	chr5:172602845-172603197	P	NEURL1B	38066
ICR_358	chr5:176785238-176785536	P	UNC5A	25023
ICR_360 <sup>^</sup>	chr5:179167525-179167654	M	ADAMTS2	0
ICR_366* <sup>^</sup> #	chr6:3848794-3850307	M	FAM50B	0
ICR_376	chr6:27827550-27827724	M	H4C11	3070
ICR_380	chr6:28742326-28742467	M	RPSAP2	9352
ICR_385 <sup>^</sup>	chr6:30781799-30782146	P	HCG20	0
ICR_393 <sup>^</sup>	chr6:39367315-39368095	P	KIF6	0
ICR_394 <sup>^</sup>	chr6:41627093-41627387	P	MDFI	9631
ICR_404 <sup>^</sup> #	chr6:144006941-144008825	M	PLAGL1 HYMAI	0
ICR_407	chr6:149986298-149986661	P	BTF3P10	7609
ICR_409	chr6:160005401-160005610	M	IGF2R AIRN	0
ICR_410 <sup>^</sup>	chr6:160006184-160006584	M	IGF2R AIRN	0
ICR_414 <sup>^</sup>	chr6:167341434-167342866	P	TLL2	0
ICR_416 <sup>^</sup>	chr6:167667943-167668201	P	LINC02538	0
ICR_418*	chr6:168417326-168417653	P	SMOC2	23,500
ICR_420* <sup>^</sup>	chr6:169421049-169421128	P	WDR27	5292
ICR_426 <sup>^</sup>	chr7:343522-343641	P	FOXL3	52,034
ICR_427 <sup>^</sup>	chr7:360518-360693	P	FOXL3	69,030
ICR_432	chr7:1663342-1663514	M	ELFN1	2561

(Continued)

Table 1. (Continued).

ID	Genomic Coordinates	Parental Origin of Methylation	Nearest Transcript	Distance to Nearest Transcript
ICR_436*^	chr7:3089399-3089604	P	CARD11	45,532
ICR_439*^	chr7:5144439-5144757	M	ZNF890P	0
ICR_443^	chr7:23490490-23491453	M	RPS2P32	0
ICR_450	chr7:39834493-39834768	M	SSBP3P1	0
ICR_451^	chr7:41990814-41991507	P	GLI3	0
ICR_452^	chr7:45564015-45564354	P	ADCY1	9786
ICR_453^	chr7:47576623-47576932	P	TNS3	0
ICR_454*^#	chr7:50781638-50783354	M	GRB10	0
ICR_468^	chr7:67772905-67773321	P	MTCO3P41	144,556
ICR_469	chr7:69233760-69233973	P	MTCO2P25	96,725
ICR_474*^	chr7:76499727-76499956	M	DTX2	0
ICR_475*^	chr7:94656360-94658647	M	PEG10	0
ICR_481*^#	chr7:130490640-130494200	M	MEST MESTIT1	0
ICR_487^	chr7:150111840-150112171	M	ACTR3C	0
ICR_489	chr7:152910856-152911190	P	ACTR3B	0
ICR_490*^	chr7:154892532-154892702	M	DPP6	0
ICR_491	chr7:155071148-155071376	M	HTR5A	0
ICR_492	chr7:155383638-155384080	P	BLACE	15705
ICR_500	chr7:159112595-159112828	M	VIPR2	0
ICR_503	chr8:882678-883012	M	DLGAP2	0
ICR_505^	chr8:1373020-1373561	M	DLGAP2	0
ICR_506*^	chr8:1548800-1548981	M	DLGAP2	0
ICR_508^	chr8:2727637-2727760	M	CSMD1	207,593
ICR_510	chr8:8703090-8703190	M	CLDN23	0
ICR_515	chr8:22118860-22119045	P	HR	0
ICR_516	chr8:22696910-22697886	P	EGR3	3430
ICR_518*^	chr8:27472461-27472768	P	CHRNA2	0
ICR_522^	chr8:37699369-37699633	M	ZNF703	0
ICR_523^	chr8:37747687-37748265	M	ERLIN2	0
ICR_534*^	chr8:60713942-60714366	M	CHD7	0
ICR_539*^	chr8:94119578-94120523	M	CDH17	6639
ICR_541*^	chr8:101277219-101278202	P	LINC02844	14,243
ICR_542*^	chr8:102528555-102528786	P	ODF1	22,803
ICR_548*^	chr8:140098048-140100981	M	TRAPPC9 PEG13	0
ICR_549	chr8:140349279-140349564	M	TRAPPC9	0
ICR_550	chr8:141723822-141724064	P	MROH5	216,592
ICR_553	chr8:143399766-143399977	P	RHPN1	15,545
ICR_555^	chr8:143728031-143728348	M	FAM83H	0
ICR_561^	chr9:21997429-22000964	P	CDKN2B	1939
ICR_562*^	chr9:35036051-35036291	M	C9orf131	4804

(Continued)

**Table 1.** (Continued).

ID	Genomic Coordinates	Parental Origin of Methylation	Nearest Transcript	Distance to Nearest Transcript
ICR_563	chr9:37800197-37800386	M	DCAF10	168
ICR_564	chr9:38487573-38487989	M	TCEA1P3	8029
ICR_570	chr9:41267302-41267410	M	PTGER4P1	12,049
ICR_578	chr9:62844696-62844981	M	CDK2AP2P2	0
ICR_598^	chr9:84272060-84272363	M	SLC28A3	760
ICR_600	chr9:87944657-87944766	M	SPATA31C1	21,000
ICR_601^	chr9:89282235-89282503	M	CKS2	28,692
ICR_603^	chr9:95313103-95313511	M	FANCC	0
ICR_604*^	chr9:96177087-96177730	P	EIF4BP3	29,122
ICR_609*^	chr9:117642714-117642890	M	RPL35AP22	42,368
ICR_616^	chr9:128415922-128416668	P	CERCAM	0
ICR_617	chr9:130327055-130327332	P	HMCN2	0
ICR_620^	chr9:134626633-134626781	P	COL5A1	15,008
ICR_623	chr9:135605044-135605311	P	PAEPP1	13,151
ICR_625^	chr9:136656981-136657090	P	HSPC324 EGFL7	0
ICR_626	chr9:137145779-137145957	P	GRIN1	0
ICR_627^	chr9:137306698-137307023	P	EXD3	0
ICR_630*^	chr10:789268-789465	P	LARP4B	17449
ICR_633^	chr10:5645451-5645631	P	ASB13	0
ICR_640^	chr10:18261294-18261435	M	CACNB2	0
ICR_641^	chr10:24519852-24520359	M	KIAA1217	0
ICR_643*^	chr10:27413523-27414477	M	PTCHD3	0
ICR_644^	chr10:28326170-28327001	P	ZNF101P1	12,276
ICR_664^	chr10:71266448-71266685	P	UNC5B	0
ICR_665^	chr10:71279400-71279528	P	UNC5B	0
ICR_666^	chr10:78356394-78357287	P	LINC00595	76,181
ICR_667^	chr10:80136121-80136538	P	PLAC9	0
ICR_674^	chr10:97974158-97974573	M	CRTAC1	0
ICR_675	chr10:100669022-100669173	P	PAX2	66,223
ICR_679	chr10:104275410-104275792	M	GSTO2	0
ICR_681*^	chr10:119817943-119819030	M	INPP5F	0
ICR_686*^	chr10:126882020-126882047	P	DOCK1	23,362
ICR_687^	chr10:127911380-127911781	P	PTPRE	0
ICR_689^	chr10:130301062-130301272	M	LINC02646	0
ICR_693	chr10:133099321-133099567	P	ADGRA1	0
ICR_694	chr10:133246176-133246423	P	MIR202HG	56
ICR_695	chr10:133569810-133570081	M	SPRNP1	0

(Continued)

Table 1. (Continued).

ID	Genomic Coordinates	Parental Origin of Methylation	Nearest Transcript	Distance to Nearest Transcript
ICR_703	chr10:133740759-133740834	M	DUX4L29	0
ICR_708*^	chr11:396655-396870	P	PKP3	0
ICR_709*^	chr11:397385-397461	P	PKP3	0
ICR_711	chr11:420604-420662	M	ANO9	0
ICR_716*^#	chr11:1997886-1999417	P	MRPL23 H19	0
ICR_717*^#	chr11:1999793-2000383	P	MRPL23 H19	0
ICR_718*^#	chr11:2000487-2001247	P	MRPL23 H19	0
ICR_719*^#	chr11:2001655-2003118	P	MRPL23	0
ICR_720*^#	chr11:2698157-2699485	M	KCNQ1 KCNQ1OT1	0
ICR_721*^#	chr11:2699814-2701210	M	KCNQ1 KCNQ1OT1	0
ICR_724*^	chr11:7088963-7089048	M	NLRP14 RBML2	0
ICR_726^	chr11:14259048-14259382	M	SPON1	0
ICR_730	chr11:44328419-44329478	P	ALX4	18,280
ICR_737*^	chr11:62371153-62371400	M	ASRGL1	0
ICR_751*^	chr11:119942219-119942412	P	LINC02744	45,533
ICR_752*^	chr11:119982974-119983610	P	LINC02744	4335
ICR_755^	chr11:132792676-132793068	M	OPCML	0
ICR_756	chr11:133081840-133082221	M	OPCML	0
ICR_757	chr11:133222318-133222823	P	OPCML	0
ICR_767	chr12:31120459-31120874	M	OVOS2	0
ICR_779	chr12:49543394-49543481	P	KCNH3	0
ICR_782	chr12:52321080-52321266	M	KRT83	0
ICR_784*^	chr12:55996580-55996638	M	RAB5B SUOX	0
ICR_789^	chr12:92503489-92504056	P	LINC02397	19,542
ICR_795	chr12:110501049-110501164	M	VPS29	0
ICR_799^	chr12:124259431-124259804	P	RFLNA	29360
ICR_802^	chr12:124759333-124759536	P	SCARB1	17,320
ICR_807*	chr12:132436944-132437228	P	MUC8	34,343
ICR_809	chr12:132603392-132603498	M	LRCOL1	0
ICR_814	chr13:20142811-20142911	M	GJA3	0
ICR_818*^	chr13:21242471-21243094	P	LINC01046	7267
ICR_825	chr13:48317373-48317679	M	RB1 PPP1R26P1	0
ICR_826#	chr13:48317894-48321417	M	RB1 PPP1R26P1	0
ICR_827*^	chr13:60267612-60268519	M	LINC00434	0
ICR_829^	chr13:80654682-80655272	M	PWWP2AP1	125
ICR_835	chr13:110813578-110813640	M	LINC00567	494
ICR_836	chr13:111411595-111411773	M	TEX29	67,347
ICR_838^	chr13:113729641-113730537	P	GRK1	0
ICR_853	chr14:33799786-33799948	M	NPAS3	0
ICR_854	chr14:35825391-35825732	M	BRMS1L	0

(Continued)

**Table 1.** (Continued).

ID	Genomic Coordinates	Parental Origin of Methylation	Nearest Transcript	Distance to Nearest Transcript
ICR_859^	chr14:74265554-74265792	P	VSX2	2816
ICR_866^	chr14:96588928-96589205	P	PAPOLA	21812
ICR_869^	chr14:100714137-100714444	P	DLK1	12,421
ICR_871^	chr14:100810929-100811087	P	MIR2392	3404
ICR_873*^#	chr14:100824556-100828242	S	MEG3	0
ICR_875*^	chr14:104171069-104171501	M	KIF26A	0
ICR_878^	chr14:105060530-105060974	P	GPR132	0
ICR_879	chr14:105628650-105629100	P	IGH	0
ICR_887^#	chr15:23647239-23648622	S	MAGEL2	0
ICR_888#	chr15:23686523-23686574	S	NDN	0
ICR_893*^	chr15:24954592-24956828	M	SNHG14 SNRPN SNURF	0
ICR_898*^	chr15:40769605-40770075	P	DNAJC17 C15orf62	0
ICR_907^	chr15:66877196-66878321	P	LINC02206	53,216
ICR_909^	chr15:70605464-70606129	P	SALRNA3	9418
ICR_912^	chr15:95287058-95287471	P	LINC01197	0
ICR_913^	chr15:98865375-98866277	M	IGF1R	0
ICR_914^	chr15:99476322-99476786	P	LINC02244	73,869
ICR_917	chr16:159416-159850	P	HBZP1	3217
ICR_919	chr16:801561-801834	P	GNG13	827
ICR_920	chr16:817208-818000	M	PRR25	3347
ICR_921^	chr16:1043980-1044213	P	SSTR5	28,543
ICR_926^	chr16:3431819-3432009	M	ZNF597	405
ICR_928	chr16:5490312-5490585	M	RBFOX1	0
ICR_930*	chr16:14990248-14990306	M	PDXDC1	0
ICR_946	chr16:33808459-33808588	P	ENPP7P13	24,184
ICR_956*	chr16:35271909-35272955	P	C2orf69P5	7713
ICR_957	chr16:35397156-35398017	P	LINC01566	5443
ICR_962*^	chr16:46757358-46757691	P	MYLK3	0
ICR_964^	chr16:57889831-57890669	P	CNGB1	0
ICR_982	chr17:1961067-1961305	P	RTN4RL1	0
ICR_990	chr17:16856437-16856709	P	COTL1P1	316
ICR_999	chr17:21685888-21686090	M	KCNJ18	6433
ICR_1006	chr17:34040220-34040257	M	ASIC2	0
ICR_1010^	chr17:40014561-40014758	P	CSF3	682
ICR_1020^	chr17:50639135-50639654	P	ABCC3	0
ICR_1024*^	chr17:76079666-76079946	P	ZACN	0
ICR_1025^	chr17:76542972-76543727	P	CYGB PRCD	0
ICR_1027	chr17:79517963-79518428	P	RBFOX3	0
ICR_1028^	chr17:80191857-80192326	P	CARD14	0
ICR_1036^	chr18:13379767-13380531	P	LDLRAD4	0
ICR_1038	chr18:37258900-37259288	P	CELF4	0
ICR_1039	chr18:47526284-47526407	M	MIR4527HG	0
ICR_1048^	chr18:79616752-79617334	M	CTDP1	62,469
ICR_1051	chr18:79638645-79638833	M	CTDP1	40,970
ICR_1052^	chr18:80147168-80147833	M	ADNP2	6822
ICR_1053^	chr18:80147992-80149033	M	ADNP2	7646
ICR_1054*^	chr19:386289-386791	P	THEG	9596
ICR_1062	chr19:1779885-1780102	P	ONECUT3	0

(Continued)



Table 1. (Continued).

ID	Genomic Coordinates	Parental Origin of Methylation	Nearest Transcript	Distance to Nearest Transcript
ICR_1068^	chr19:3006289-3006627	M	TLE2	0
ICR_1079	chr19:6509209-6509630	P	TUBB4A	6361
ICR_1083	chr19:7863802-7864121	M	EVI5L	0
ICR_1085	chr19:9912721-9912951	M	OLFM2	0
ICR_1086*^	chr19:9953808-9954321	P	COL5A3	5240
ICR_1091*^	chr19:14061704-14062308	P	PALM3	0
ICR_1093	chr19:15777135-15778369	P	CYP4F24P	0
ICR_1095	chr19:15940417-15941089	P	CYP4F11	5551
ICR_1099*	chr19:19120808-19121015	M	TMEM161A	0
ICR_1101*^	chr19:19997705-19997967	P	BNIP3P12	0
ICR_1107^	chr19:29662034-29662704	P	PLEKHF1	2718
ICR_1109^	chr19:33298571-33298842	P	CEBPA	1092
ICR_1120	chr19:43406341-43406626	M	TEX101	0
ICR_1129	chr19:50489534-50489611	M	EMC10	0
ICR_1135*^	chr19:53537445-53538957	M	ZNF331	0
ICR_1136^	chr19:53553906-53554999	M	ZNF331	0
ICR_1141^	chr19:56478788-56479078	M	ZNF667	723
ICR_1142*^#	chr19:56837320-56841439	M	ZIM2 PEG3 MIMT1	0
ICR_1149^	chr20:890832-892113	P	ANGPT4	0
ICR_1155^	chr20:23164173-23164463	P	RNA5SP478	3202
ICR_1161	chr20:29325493-29325868	M	DUX4L33	444
ICR_1190^	chr20:31496438-31497008	P	LINC00028	8864
ICR_1191*^	chr20:31547027-31548129	M	HM13 MCTS2P	0
ICR_1192^#	chr20:37520202-37521842	M	BLCAP NNAT	0
ICR_1193^#	chr20:37522341-37522993	M	BLCAP NNAT	0
ICR_1194*^#	chr20:43513725-43515256	M	L3MBTL1	0
ICR_1205*^#	chr20:58839107-58842875	M	GNAS	0
ICR_1206*^#	chr20:58850158-58852357	M	GNAS	0
ICR_1207*^	chr20:58853850-58856828	M	GNAS	0
ICR_1209*^	chr20:59220788-59221858	M	ZNF831	0
ICR_1211	chr20:62581580-62581898	P	RPL7P3	8195
ICR_1213	chr20:63003240-63003541	P	BHLHE23	2386
ICR_1216	chr20:63474459-63475096	P	KCNQ2	1804
ICR_1315*^	chr21:29155405-29155931	M	MAP3K7CL	0
ICR_1321*^	chr21:42063975-42064308	P	UMODL1	0
ICR_1327^	chr21:45359946-45360583	P	MTCO1P3	15,608
ICR_1355*^	chr22:18967907-18968273	P	DGCR5	2225
ICR_1356^	chr22:19749148-19749533	P	TBX1	7170
ICR_1366	chr22:31104622-31104758	M	SMTN	0
ICR_1372	chr22:39664168-39664319	M	CACNA1I	0
ICR_1374^	chr22:40040395-40041632	P	FAM83F	0
ICR_1375^	chr22:41681861-41682938	M	SNU13	0
ICR_1377*^	chr22:42532792-42533280	P	RRP7A	12996
ICR_1378	chr22:42547749-42547909	P	SERHL2	5941
ICR_1384	chr22:45877926-45878087	P	ATXN10	32,619
ICR_1385*	chr22:48238911-48239473	P	MIR3201	34,891
ICR_1394	chrX:2325208-2325958	M	DHRX	0
ICR_1395^	chrX:2962476-2962843	P	ARSL	0
ICR_1398	chrX:11138801-11139297	M	ARHGAP6	0
ICR_1399*^	chrX:14244065-14244239	M	UBE2E4P	26
ICR_1400*	chrX:17655055-17655175	M	NHS	0
ICR_1408*	chrX:38474430-38475389	P	FTLP16	9372

(Continued)

**Table 1.** (Continued).

ID	Genomic Coordinates	Parental Origin of Methylation	Nearest Transcript	Distance to Nearest Transcript
ICR_1413 <sup>^</sup>	chrX:40243438-40244131	P	BCOR	66048
ICR_1417 <sup>*^</sup>	chrX:47637837-47638168	M	ELK1	0
ICR_1441 <sup>^</sup>	chrX:99939597-99940400	M	B3GNT2P1	51,491
ICR_1468 <sup>^</sup>	chrX:133437318-133438444	P	GPC4	21,829
ICR_1484 <sup>^</sup>	chrX:154408925-154409317	P	DNASE1L1	0

Regions of differential methylation meeting criteria reported herein for ICRs that overlap with regions of gamete-specific methylation. Parental allele methylated indicates which gamete source showed hypermethylation – Paternal (P – sperm) or Maternal (M – oocyte) based upon both sperm and oocyte methylation data. Previously reported ICRs that do not have gamete specific methylation are also included and labelled as having Somatic (S) methylation. ICRs overlapping ENCODE annotated regions of CTCF binding and DNase I hypersensitivity are indicated by \* and <sup>^</sup>, respectively. ICRs overlapping previously published ICRs of imprinted genes are indicated by #.

<sup>+</sup>Criteria for an ICR: 1)  $\geq 5$  consecutive CpG sites, 2) methylation levels of  $50\% \pm 15\%$ , 3) similarity of methylation levels in tissues from the three germ layers (i.e., brain, liver, and kidney), and 4) similarity of methylation across individuals.

defined, at least in part, by the present human imprintome. For example, the ICRs for *ZDBF2* (ICR\_165-176) are shown in Supplementary Figure S2A. An ICR for the tumour suppressor gene *IGF2R* [31] (ICR\_409, 410) is found only in intron 2 in humans (Supplementary Figure S2B). This is similar to what has been observed in the dog [32], but different from that observed in the mouse, which also has an ICR in the promoter region [33].

We also identified novel candidate ICRs mapping near *PTCHD3* (ICR\_643, Figure 2(c), Table 1) and *MCTS2P/HM13* (ICR\_1191, Figure 2(d)), (Table 1). Other novel candidate ICRs include those mapping near *WNT10A* (ICR\_177, Supplementary Figure S3A, Table 1) and *ADNP2/PARD6G* (ICR\_1052, 1053, Supplementary Figure S3B, Table 1). Such findings indicate the presence of additional imprinted genes in the human genome.

### Similarity of methylation marks across accessible tissues

For diagnostics and public health screening, it is critically important that DNA methylation marks be reproducible using other sequencing technologies and be similar to that in otherwise healthy human's accessible tissues (e.g., peripheral blood, maternal or foetal tissues discarded at birth (e.g., placenta), or HUVECs). These tissues also often serve as controls in epidemiologic

studies, and act as surrogates for affected inaccessible tissues.

To assess reproducibility, we selected two well-characterized ICRs regulating the imprinted expression of *PEG3/ZIM2* (ICR\_1142, Figure 3(a)), (Table 1) and Supplementary Table S1) and *PEG10* (ICR\_475, Figure 3(b), Table 1 and Supplementary Table S1) for which we were also able to develop pyrosequencing assays using the PCR primer sets provided in Supplementary Table S3 to determine DNA methylation levels. We used pyrosequencing to test whether CpG methylation averaged 50% in these canonical ICRs samples. The DNA methylation patterns determined with pyrosequencing of embryonic brain, kidney, and liver fell between 35% and 65% and averaged approximately 50%. This was comparable to that found with WGBS in these well-characterized ICRs (Figure 3(c,d)).

Samples of internal tissues are generally unavailable for research, diagnostics or public health screening purposes. To determine if methylation marks at known ICRs are similar in accessible tissues from healthy individuals, we again characterized ICRs regulating the imprinted expression of *PEG3/ZIM2* (ICR\_1142, Figure 3(a)), (Table 1) and Supplementary Table S1) and *PEG10* (ICR\_475, Figure 3(b), Table 1 and Supplementary Table S1) in CD14<sup>-</sup> monocytes from newborn cord blood and HUVECs. The methylation patterns determined with pyrosequencing were comparable to those found with WGBS

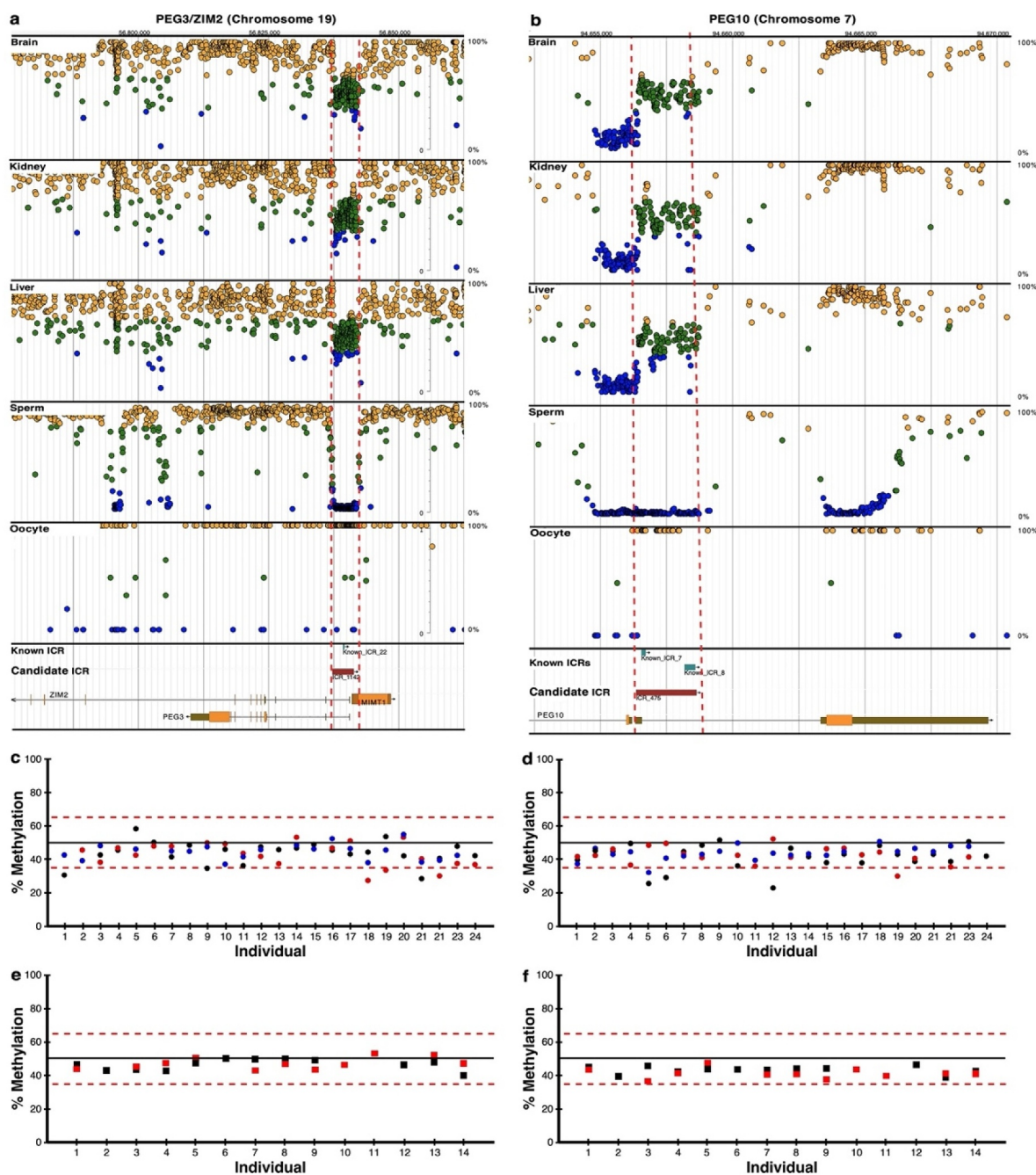


**Figure 3.** Pyrosequencing results for previously known ICRs. DNA methylation profiles determined by whole genome bisulphite sequencing (WGBS) are shown for imprinted genes (a) *PEG3/ZIM2* (ICR\_1142) and (b) *PEG10* (ICR\_475) with previously known (blue boxes) and candidate ICRs (red boxes); visualize at <https://humanic.org/>. DNA methylation levels determined by WGBS in sperm and oocytes are also provided. These sequence data were supplemented with publicly available gametic sequence (accession number JGAS0000000006) and part of control sperm data from PRJNA754049 [25,26]. Dots indicate hemi-methylation (green), hypomethylation (blue) and hypermethylation (yellow) based on (WGBS). The vertical dashed red lines delineate the candidate ICR regions. Confirmation of  $50 \pm 15\%$  DNA methylation of the ICRs determined by WGBS is shown for (c) *PEG3/ZIM2* and (d) *PEG10* using pyrosequencing of kidney (black circles), liver (red circles), and brain (blue circles) tissues from 24 embryos. Confirmation of  $50 \pm 15\%$  DNA methylation determined by WGBS is shown for (e) *PEG3/ZIM2* and (f) *PEG10* using pyrosequencing for CD14 monocytes (red squares) and HUVECs (black squares) from 14 adult individuals.

in these well-characterized ICRs in the CD14<sup>-</sup> monocytes and HUVECs (Figure 3(e,f)), falling between 35% and 65% methylation and averaging

50% in these accessible tissues as expected for *bona fide* ICRs. These results indicate that accessible peripheral tissues can be used to assess the effects

on the human imprintome from early life exposures to chemicals, physical agents (e.g., radiation, blunt force trauma, heat stress, etc.), and other adverse physiological conditions.

### **Novel ICR methylation and human pathology**

Many of the novel ICRs identified are in regions previously implicated in the pathogenesis of human diseases. For example, four candidate differentially methylated ICRs are located within the Down syndrome (DS) critical region at chromosome 21q22 [34]. ICR\_1317 resides in the promoter of *HLCS* (Supplementary Figure S4A, Supplementary Table S1); ICR\_1318 is in intron 1 of *RIPPLY3* (Supplementary Figure S4A, Supplementary Table S1); ICR\_1319 is close to the 3' UTR of *KCNJ6* (Supplementary Figure S4B, Supplementary Table S1); and ICR\_1320 is in intron 1 of *GET1* (Supplementary Figure S4C, Supplementary Table S1).

The functions of these genes have developmental implications, playing roles in the metabolism required for infant growth and development (*HLCS*); transcriptional regulation controlling pharyngeal development (*RIPPLY3*); cell membrane potential regulating G-protein coupled receptors in both cardiac and neuronal signalling, with mutations connected to developmental delay with facial abnormalities and intellectual phenotypes (*KCNJ6*); and intracellular transport and positioning of proteins involved in signal transduction pathways connected to retinal deterioration and nystagmus (*GET1*).

Interestingly, ICR\_1319 and the highly restricted Down syndrome critical region (HR-DSCR) of only 34 kb [35] flank *KCNJ6* on distal 21q22.13, suggesting that not only gene duplication but also imprinting dysregulation may be involved in DS. Moreover, the first intron of the *GET1* gene harbours a single nucleotide polymorphism (rs2244352, chr21:39,386,047) (Supplementary Figure S4C) implicated in comitant esotropia, a condition resulting in poor binocular vision that affects ~20% of Down syndrome cases. The SNP rs2244352 is associated with risk in a parent-of-origin dependent manner, with significant association between incidence and paternal

inheritance of the minor 'T' allele [36,37]. The major allele for rs2244352 is G. Thus, carrying the minor T allele would eliminate the formation of a CG dinucleotide able to be methylated; however, loss of methylation on the paternal chromosome is likely not the causative mechanism.

It has been shown that this region is differentially methylated, but that it is the maternal allele that is methylated [36]. Our gametic data is also consistent with maternal methylation, showing hypomethylation in sperm and hypermethylation in oocytes (Supplementary Figure S4C). With no loss of paternal methylation possible to cause dysregulation of this putative ICR, we hypothesize an alternate mechanism, in which repressor binding occurs on unmethylated CG sites in this region. This would be comparable to regulation at the *H19/Igf2* ICR, by CTCF binding of the unmethylated allele [14]. Thus, if 'CG' to 'TG' substitution alters the recognition sequence for repressor binding, paternal *GET1* expression could be activated, adding to the expression from the maternal copy protected from repression by methylation of the putative ICR.

Similarly, four candidate ICRs are located within the DiGeorge syndrome critical region at chromosome location 22q11.2 (Supplementary Figure S5 A, C) [38,39]. Hemizygous microdeletions in this crucial region result in developmental disorders, such as velopharyngeal insufficiency, variable conotruncal heart defects, and cognitive and behavioural disorders (e.g., schizophrenia, bipolar disorder, and autism) [38]. Moreover, differential brain effects have been reported with the maternal or paternal deletion of 22q11.2, suggesting a role of imprinted genes in the aetiology of these psychiatric abnormalities [38]. The ICRs identified are ICR\_1355 in the promoter of *DGCR5* (Supplementary Figure S5A, Supplementary Table S1); ICR\_1356 is in the promoter region of *TBX1* and ICR\_1357 is intronic (Supplementary Figure S5B, Table 1 and Supplementary Table S1). ICR\_1358, which overlaps pseudogene *ABHD17AP4* (Supplementary Figure S5C, Supplementary Table S1), is upstream of *SERPIND1* and *SNAP29* (Supplementary Table S1). Functionally, *DGCR5* is a long non-coding RNA that acts as a regulator of apoptosis and proliferation; *TBX1* is a transcription factor



involved in the regulation of developmental processes, with its deletion directly linked to physical malformations seen in DiGeorge syndrome; *SERPIND1* is a protease inhibitor with critical functions in blood clotting; and *SNAP29* is a member of a family of synaptic vesicle trafficking regulators associated with developmental disorders of the CNS.

We previously used a computer algorithm to predict the genome-wide imprint status of human genes from sequence features [19]. *DLGAP2* was predicted to be imprinted and demonstrated to be paternally expressed. It is a membrane-associated protein that plays a role in synapse organization and signalling in neuronal cells. It was subsequently implicated in autism based upon CNV analyses [40]. In this study, we identified an ICR\_502 in intron 1 (Supplementary Figure S6A, Supplementary Table S1); this gene also contains ICR\_503-506 (Table 1 and Supplementary Table S1). Thus, the function of *DLGAP2* could potentially be altered both genetically and epigenetically in the formation of autism. Interestingly, of the 102 annotated genes we predicted with the use of computer algorithms to be imprinted [19], we have now identified ICRs for 35 of them (34%) (Supplementary Table S1 and Supplementary Table S4), providing additional supporting evidence that they are imprinted.

*PRDM16* functions as a transcription coregulator in the development of brown adipocytes and increased expression may protect against obesity [41]. We previously predicted it to be imprinted and paternally expressed in both mice [42] and humans [19]. Interestingly, ICR\_11 and ICR\_12 (Supplementary Table S1), while overlapping *TTC34*, are also within 500kb of *PRDM16*. Although the oocyte methylation data are sparse, it appears that the paternal allele at these ICR regions is sparsely or entirely unmethylated while the maternal allele is methylated, suggesting that *PRDM16* is paternally expressed as predicted by Luedi *et al.* [19]. Using less stringent criteria (i.e., 50 + 20% DNA methylation), there is also an ICR in the promoter region of *PRDM16* (ICR\_3070\_54) and three additional intronic ICRs (i.e., ICR\_3070\_55-57; Supplementary Figure S6B). Should this gene be experimentally confirmed to be imprinted, genomic imprinting

would be involved in the maturation of both white [43] and brown fat cells, making the role of imprinted gene expression in metabolism and obesity more extensive than previously appreciated.

Imprinted genes have been identified on the X-chromosome in mice [44], but not in humans. Nevertheless, we have identified 98 putative ICRs on the X-chromosome (ICR\_1391-1488, Supplementary Table S1), indicating that imprinted genes are also present on the human X chromosome. Gamete DNA methylation was adequate to determine parent-of-origin methylation for 11 of these ICRs (6 maternally methylated and 5 paternally methylated, Table 1). Only *DHRSX* (ICR\_1394), a secretory protein associated with starvation-induced autophagy [45], is located in a pseudoautosomal region – PAR1 (Figure 4). The role of these candidate imprinted genes in the genesis of parental-dependent behavioural disorders, such as those observed in Turner syndrome [46] needs further investigation.

### Functional significance of ICR methylation

*Bona fide* ICRs typically regulate gene expression by controlling access to transcriptional regulatory sites within the imprinted genes. We examined the overlap of our 1,488 candidate ICRs with DNase I hypersensitive sites, regulatory motifs, and transcription factor-binding sites for nearby genes. Of the 332 ICRs that were either unmethylated or fully methylated in gametes, 200 (60%) overlapped with DNase I hypersensitive regions. Of those 332 ICRs, 178 were hypermethylated in sperm DNA sequences, and 154 were hypermethylated in oocytes.

Moreover, for each ICR, we looked for regulatory motifs within  $\pm 5,000$  bp using Analysis of Motif Enrichment (AME) [47] against the Homo Sapiens Comprehensive Model Collection (HOCOMOCO). This consists of motifs for 680 known transcription factors. Approximately one-third of the 680 known transcription factor-binding sites are within or near candidate ICRs, supporting the functional significance of these ICRs (Supplementary Table S5).

The limited number of ICRs previously characterized [14] are over-selected for growth effectors,



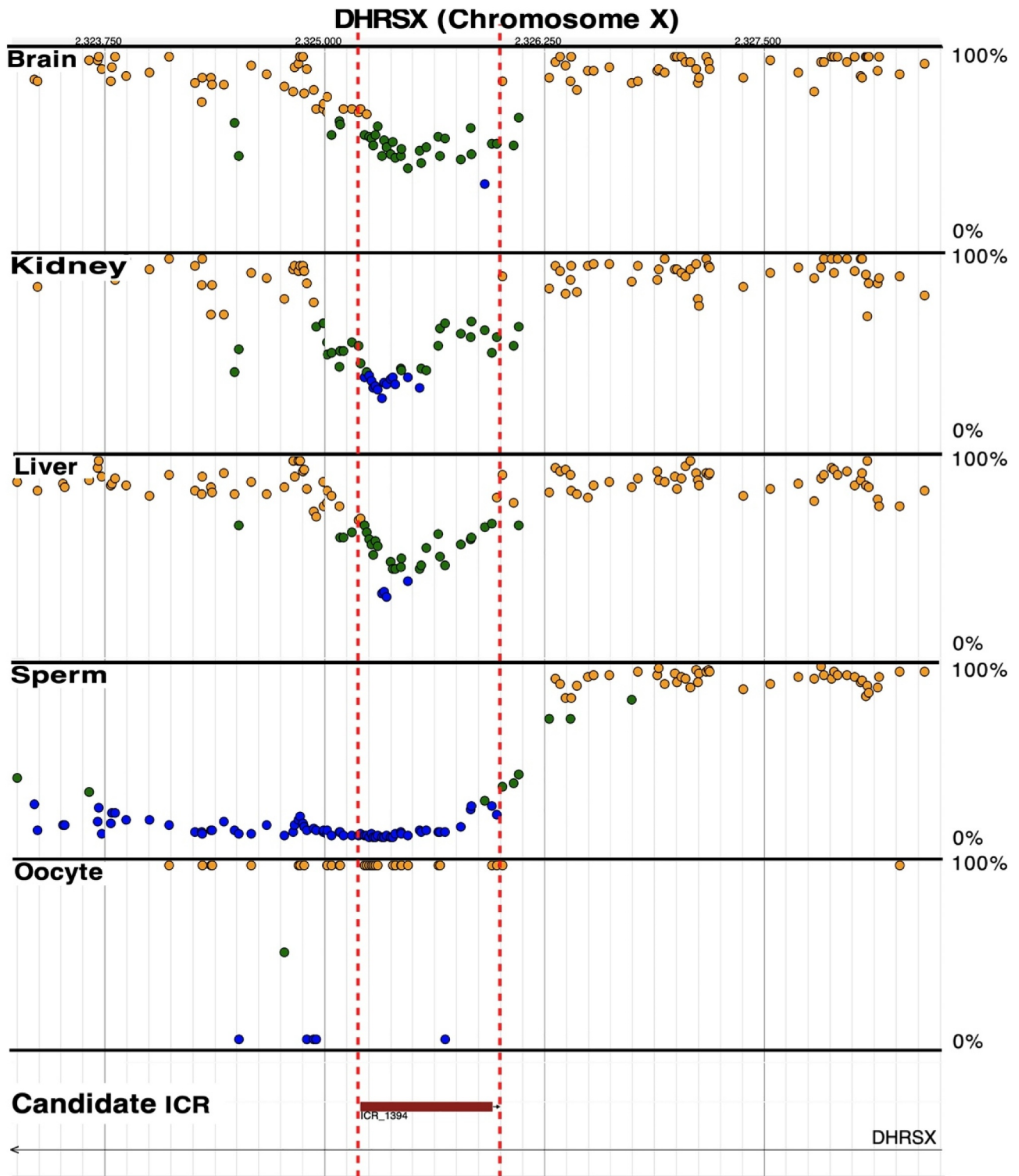


**Figure 4.** Candidate ICR for *DHRSX* (ICR\_1394) in the pseudo autosomal region, PAR1, on the X chromosome; visualize at <https://humanicr.org/>. Whole genome bisulphite sequencing (WGBS) identified a candidate ICR (red box) in embryonic brain, kidney, and liver tissue for a candidate imprinted gene associated with starvation induced autophagy [45]. DNA methylation determined by WGBS in sperm and oocytes is also shown; these sequence data were supplemented with publicly available gametic sequence (accession number JGAS0000000006) and part of control sperm data from PRJNA754049 [25,26]. Dots indicate hemi-methylation (green), hypomethylation (blue) and hypermethylation (yellow) based on WGBS. The vertical dashed red lines delineate the candidate ICR regions.

with dysregulation associated with a wide range of conditions, including metabolic disorders, cancers, neurological diseases, language development deficits, schizophrenia, and bipolar affective disorders [48,49]. Thus, we examined the predicted functions of the 914 genes associated with the 332 candidate ICRs with gamete-specific methylation (Supplementary Table S6) by performing gene ontology (GO) analysis using Gorilla (<http://cbl-gorilla.cs.technion.ac.il/>) (Supplementary Table S7). The most significant high-level biological processes identified by Gorilla were cAMP biosynthetic processes, cellular response to glucagon, and adenylate cyclase-activating G protein-coupled receptor signalling pathway (Supplementary Table S7). Functional analysis of candidate regions using the Comparative Toxicogenomics Database (CTD) identified protein-binding and DNA-binding as enriched GO terms in the functional annotations (Supplementary Table S8). Of the top five pathways identified by Ingenuity Pathway Analysis (IPA) (QIAGEN Inc., <https://www.qiagenbioinformatics.com/products/ingenuity-pathway-analysis>), three were important neurological pathways: gonadotropin-releasing hormone (GnRH) signalling, endocannabinoid neuronal synapse pathway, and g-aminobutyric acid receptor signalling (Supplementary Table S9). Five hundred eight genes were associated with neurological disease, while 168 were related to nervous system development and function. Of the top networks identified by IPA, RNA post-transcriptional modification, cell cycle and DNA replication, recombination, and repair had the highest score, with auditory disease, cellular compromise, and neurological disease coming in second. Results of KEGG and REACTOME analysis of enriched pathways included neuronal system, transmission across chemical synapses, signal transduction, pathways in cancers, circadian entrainment, axon guidance, cholinergic synapse, glutamatergic synapse, and calcium signalling pathways (Supplementary Table S10) [50].

We also explored the role of the candidate imprinted genes in human disease using the Mouse Genome Informatics (MGI) database and the CTD and their curation of OMIM disease categories and inferred diseases via chemical-gene

chemical-disease associations [51]. Consistent with the preceding analyses, several neurological disorders correlated with a subset of the genes in MGI, including Alzheimer's disease ( $n = 2$ ), autism spectrum disorder ( $n = 6$ ), various ataxias, and cranial developmental disorders. When inferred disease associations were factored into the CTD analysis, the number of gene-disease associations restricted to neurological disorders expanded greatly, e.g., 242 genes were associated with Alzheimer's disease and 243 with Parkinson's disease. For Alzheimer's disease, 16 of the 242 genes were unique to the disorder (*ABHD17AP4*, *BRE*, *C2ORF27A*, *CCDC144B*, *CERS3*, *CUTALP*, *DHRXS*, *DUX4L1*, *FAM155B*, *FRG1CP*, *FRG2B*, *GPR78*, *HERC2P4*, *JRKL*, *KBTBD13*, *KCNAB1*); whereas, for Parkinson's disease, 17 were unique (*ADARB2*, *AFF2*, *CDH24*, *CMC4*, *CPAMD8*, *CRTC1*, *DBH-AS1*, *DIRAS3*, *DNAJC17*, *DNM1P46*, *DTX2*, *DUX4L9*, *EPHA10*, *ERAS*, *EXD3*, *HTR5A-AS1*, *HYMAI*); the remaining genes were shared by both disorders, indicating overlapping chemical mechanisms at the molecular level in the aetiology of these diseases.

## Discussion

Epigenetic mechanisms, such as DNA methylation, are believed to link adverse intrauterine exposures to adult disease susceptibility; however, supporting empirical evidence from humans has remained scarce because of a lack of recognizable and archivable patterns of early epigenetic effects that can be detected and quantified in the epigenome [52–54]. This is especially important for human studies that rely on DNA from sample types accessible in otherwise healthy human populations (e.g., saliva or peripheral blood). While sequence regions controlling the monoallelic expression of imprinted genes have been previously proposed as targets for such studies [6], until now, only 25 of these regions have been described [14], with potentially hundreds more unknown.

Herein, we determined that the human imprintome is comprised of 1,488 regions with characteristics typically observed in known ICRs. Interestingly, the overlap between the 850,000 CpG sites in the Illumina Infinium Methylation EPIC microarray (Illumina, Inc., San Diego, CA,

USA) and the 22,279 CpG sites in the human imprintome is only 7%. Using genomic DNA obtained from three tissue types isolated from embryos of both sexes and at least two ethnicities, these regions include most of the previously identified ICRs [14]. Of the 1,488 regions, 332 also exhibited parent-of-origin specific methylation – the hallmark of an ICR. Of those ICRs, 209 overlapped with DNase I hypersensitive regions. These novel ICRs have a median CpG dinucleotide content of 248, similar to the 25 previously characterized ICRs with a size range of 10 to ~4,000 bp. When an overlap was identified between a novel and a known ICR, the novel sequence typically extended beyond the boundaries of the prior reported sequence. Chromosomes frequently contain clusters of genes that are controlled by a single ICR (i.e., imprinted domains). Thus, our 200 strongest candidate ICRs, with overlapping DNase I hypersensitive sites and gamete-specific methylation, could regulate as many as 400 imprinted genes if each ICR controlled only two genes, which is commonly observed. Expanding this to include all 332 candidate ICRs with gamete-specific methylation increases the number of potentially imprinted genes to a little more than 500 or ~3% of the genome.

Many known imprinted genes have developmental functions involving the regulation of cell function and growth such as pruning of synapses and adipocyte accrual affecting the life course. Thus, ICRs are of particular interest in studying the early origins of a wide range of common chronic diseases, including neurological disorders and metabolic diseases such as obesity, type 2 diabetes, and cancers. The majority (90%) of our candidate ICRs fall within 5,000 bp of genes involved in fundamental processes, including cAMP biosynthetic processes, cellular responses to glucagon and adenylate cyclase-activating G protein-coupled receptor signalling. Notably, a large proportion of the candidate ICRs are near genes involved in metabolic and neurological diseases, consistent with the observations of previously characterized ICRs. Characterizing and experimentally confirming the complete repertoire of ICRs could lead to the development of dietary interventions and pharmacological targeting of

specific regions to advance the precision of nutritional and chemical therapies.

For example, if the candidate ICR proximal to the zinc finger transcription factor gene *PRDM16* is experimentally confirmed to be imprinted, altered methylation can be detected in any tissue as early as birth. As *PRDM16* controls the bidirectional fate decision between brown adipocytes and myoblasts [55], early detection of alteration in an imprinted ICR could provide opportunities for pharmacological or dietary manipulation to enhance the expression of *PRDM16*, preventing metabolic dysfunction, including obesity. Similarly, disposition to hypoplasia of the thymus and parathyroid glands and conotruncal cardiac malformations and schizophrenia that potentially result from imprinting disorders in the DiGeorge syndrome critical region could be identified earlier, and potentially even during gestation when interventions may be more effective.

ICRs have the unique features of the early establishment of DNA methylation marks, similarity across cell types and tissues, and stability over the lifespan. These characteristics facilitate their broad use as stable archives of early developmental exposures that may alter metabolic and other developmental and behavioural processes in adulthood [56–58]. Thus, ICRs are logical targets for evaluating the early origins of disease using accessible cell types obtained at variable ages [59–62]. A predetermined reference panel of ICRs could be vital in identifying early exposures. Their effects on DNA methylation have a wide range of potential uses, particularly in chronic disease epidemiology where relevant past exposures may be difficult to quantify. Such a predetermined reference panel could also be key in unravelling epigenetic responses to early life chemical and non-chemical stressors that result in molecular ‘wear and tear’ as reflected in methylation changes in accessible tissue, and may improve the precision and usefulness of epigenetic clocks [63,64]. The expectation that the baseline methylation fraction of ICRs is approximately 50% and is stable over time, with little epigenetic drift, also supports the use of ICR methylation as biomarkers of adult disease susceptibility at any time during the life course. Therefore, having the complete repertoire of

*bona fide* ICRs – the *imprintome* – should improve our understanding of the early origins of adult diseases.

While the use of methylation marks as exposure proxies has long been advocated, and methylation patterns of ICRs provide a rare ‘epigenetic responsive’ window to early exposures, our results should be interpreted in the context of the study limitations. Firstly, our algorithm used to identify candidate genome-wide ICRs was tested at three methylation thresholds: relaxed 30–70% ( $50 \pm 20\%$ ), moderate 35–65% ( $50 \pm 15\%$ ), and stringent 45–55% ( $50 \pm 5\%$ ). We selected the moderate set for further analysis. While this approach is pragmatic, it does not accommodate the possibility that methylation patterns defining ICR boundaries may be more fluid, requiring additional statistical and experimental interrogation of ICRs to refine the boundaries and, with that, the imprinted genes they regulate. Bioinformatic approaches such as change-point modelling that have been used in copy number variant analyses [65,66], coupled with experimental validation, could also be deployed in the future. Secondly, we have not performed clonal-allele analysis of candidate regions to definitively prove that they are *bona fide* ICRs, with methylation patterns consistent *in cis* for the parental alleles. Thus, we do not expect all candidates to overlap true ICRs; however, based on the characteristics of known ICRs, we are confident that a majority of human ICRs are captured within the 1,488 candidate ICRs.

Despite these limitations, we have used a combination of bioinformatic and sequencing approaches to provide the first draft of the complete repertoire of human ICRs – the human *imprintome*. To facilitate its use, we have also developed an online tool, the *imprintome* browser, which is linked to the UCSC Genome Browser to visualize the data at: <https://humanicr.org/>. Further refinement is needed to identify *bona fide* ICRs and their exact boundaries. This will be bioinformatically iterative and will require experimental validation. To our knowledge, however, this is the first study to create a human ICR compendium. As these sequence regions are also present in accessible peripheral blood DNA, we anticipate our data will greatly facilitate the ability

to quantify the contribution of exposures in early development to a wide range of adult-onset chronic diseases; pave the way for novel early-detection tools; and eventually reveal the molecular underpinnings of vulnerability in disease processes, especially in early life.

### Disclosure statement

No potential conflict of interest was reported by the author(s).

### Funding

This work was supported in part by National Institutes of Health grants R01HD098857 (D.A.S., C.H., R.L.J.), R01MD011746 (C. H., D.A.S., R.L.J.), R01MD011746-S1 (C.H., D.A.S., R.L.J.), and Office of Extramural Research, National Institutes of Health. R01HD098857, R01MD011746NICHD, NIMHD, NIEHS [R01HD098857, R01MD011746-S1, P30ES025128].

### Author contributions:

C.H. and R.L.J. conceived the idea and obtained funding, D. D.J., A.M.R, F.W. and J.H. contributed bioinformatics expertise, D.A.S., A.P., A.L., S.E.C, S.S.P. and M.C. contributed mechanistic expertise to advancing the thesis. All authors contributed to drafting and editing the manuscript.

### Data availability

Data will be available from the authors upon request, and at the website <https://humanicr.org/>.

### Ethics statement

These tissues were obtained from the National Institutes of Health funded Laboratory of Human Embryology at the University of Washington, Seattle, WA; they were snap frozen to preserve DNA/RNA integrity (NCSU Institutional Review Board #3565).

### ORCID

Michael Cowley  <http://orcid.org/0000-0001-8564-4224>  
Randy L. Jirtle  <http://orcid.org/0000-0003-1767-045X>

### References

- [1] Badcock C, Crespi B. Battle of the sexes may set the brain. *Nature*. 2008;454(7208):1054–1055.
- [2] Lorgen-Ritchie M, Murray AD, Ferguson-Smith AC, et al. Imprinting methylation in SNRPN and MEST1



- in adult blood predicts cognitive ability. *PLoS One*. 2019;14(2):e0211799.
- [3] Jirtle RL, Skinner MK. Environmental epigenomics and disease susceptibility. *Nat Rev Genet*. 2007;8(4):253–262.
- [4] Jirtle RL. Genomic imprinting and cancer. *Exp Cell Res*. 1999;248(1):18–24.
- [5] Jirtle RL. IGF2 loss of imprinting: a potential heritable risk factor for colorectal cancer. *Gastroenterology*. 2004;126(4):1190–1193.
- [6] Hoyo C, Murphy SK, Jirtle RL. Imprint regulatory elements as epigenetic biosensors of exposure in epidemiological studies. *J Epidemiol Community Health*. 2009;63(9):683–684.
- [7] Franks PW, McCarthy MI. Exposing the exposures responsible for type 2 diabetes and obesity. *Science*. 2016;354(6308):69–73.
- [8] Pigeyre M, Rousseaux J, Trouiller P, et al. How obesity relates to socio-economic status: identification of eating behavior mediators. *Int J Obes (Lond)*. 2016;40(11):1794–1801.
- [9] Arpon A, Milagro FI, Ramos-Lopez O, et al. Methylome-wide association study in peripheral white blood cells focusing on central obesity and inflammation. *Genes (Basel)*. 2019;10(6):444.
- [10] Bysani M, Perfilyev A, de Mello VD, et al. Epigenetic alterations in blood mirror age-associated DNA methylation and gene expression changes in human liver. *Epigenomics*. 2017;9(2):105–122.
- [11] Joubert BR, Felix JF, Yousefi P, et al. DNA methylation in newborns and maternal smoking in pregnancy: genome-wide consortium meta-analysis. *Am J Hum Genet*. 2016;98(4):680–696.
- [12] Meeks KAC, Henneman P, Venema A, et al. An epigenome-wide association study in whole blood of measures of adiposity among Ghanaians: the RODAM study. *Clin Epigenetics*. 2017;9:103.
- [13] Kessler NJ, Waterland RA, Prentice AM, et al. Establishment of environmentally sensitive DNA methylation states in the very early human embryo. *Sci Adv*. 2018;4(7):eaat2624.
- [14] Skaar DA, Li Y, Bernal AJ, et al. The human imprintome: regulatory mechanisms, methods of ascertainment, and roles in disease susceptibility. *ILAR J*. 2012;53(3–4):341–358.
- [15] Murphy SK. Targeting the epigenome in ovarian cancer. *Future Oncol*. 2012;8(2):151–164.
- [16] Murphy SK, Adigun A, Huang Z, et al. Gender-specific methylation differences in relation to prenatal exposure to cigarette smoke. *Gene*. 2012;494(1):36–43.
- [17] Cassidy FC, Charalambous M, Suarez RK. Genomic imprinting, growth and maternal-fetal interactions. *J Exp Biol*. 2018;221(Pt Suppl 1). DOI:10.1242/jeb.164517
- [18] Kitsiou-Tzeli S, Tzetis M. Maternal epigenetics and fetal and neonatal growth. *Curr Opin Endocrinol Diabetes Obes*. 2017;24(1):43–46.
- [19] Luedi PP, Dietrich FS, Weidman JR, et al. Computational and experimental identification of novel human imprinted genes. *Genome Res*. 2007;17(12):1723–1730.
- [20] Green BB, Kappil M, Lambertini L, et al. Expression of imprinted genes in placenta is associated with infant neurobehavioral development. *Epigenetics*. 2015;10(9):834–841.
- [21] Ishida M, Moore GE. The role of imprinted genes in humans. *Mol Aspects Med*. 2013;34(4):826–840.
- [22] Lambertini L, Marsit CJ, Sharma P, et al. Imprinted gene expression in fetal growth and development. *Placenta*. 2012;33(6):480–486.
- [23] Soubry A, Hoyo C, Butt CM, et al. Human exposure to flame-retardants is associated with aberrant DNA methylation at imprinted genes in sperm. *Environ Epigenet*. 2017;3(1):dvx003.
- [24] Soubry A, Murphy SK, Vansant G, et al. Opposing epigenetic signatures in human sperm by intake of fast food versus healthy food. *Front Endocrinol (Lausanne)*. 2021;12:625204.
- [25] Okae H, Chiba H, Hiura H, et al. Genome-wide analysis of DNA methylation dynamics during early human development. *PLoS Genet*. 2014;10(12):e1004868.
- [26] Schrott R, Murphy SK, Modliszewski JL, et al. Refraining from use diminishes cannabis-associated epigenetic changes in human sperm. *Environ Epigenet*. 2021;7(1):dvab009.
- [27] Lander ES, Linton LM, Birren B, et al. Initial sequencing and analysis of the human genome. *Nature*. 2001;409(6822):860–921.
- [28] Li J, Bench AJ, Vassiliou GS, et al. Imprinting of the human L3MBTL gene, a polycomb family member located in a region of chromosome 20 deleted in human myeloid malignancies. *Proc Natl Acad Sci USA*. 2004;101(19):7341–7346.
- [29] Evans HK, Wylie AA, Murphy SK, et al. The neuronatin gene resides in a “micro-imprinted” domain on human chromosome 20q11.2. *Genomics*. 2001;77(1–2):99–104.
- [30] Schulz R, McCole RB, Woodfine K, et al. Transcript- and tissue-specific imprinting of a tumour suppressor gene. *Hum Mol Genet*. 2009;18(1):118–127.
- [31] De Souza AT, Hankins GR, Washington MK, et al. M6P/IGF2R gene is mutated in human hepatocellular carcinomas with loss of heterozygosity. *Nat Genet*. 1995;11(4):447–449.
- [32] O’Sullivan FM, Murphy SK, Simel LR, et al. Imprinted expression of the canine IGF2R, in the absence of an anti-sense transcript or promoter methylation. *Evol Dev*. 2007;9(6):579–589.
- [33] Stoger R, Kubicka P, Liu CG, et al. Maternal-specific methylation of the imprinted mouse Igf2r locus identifies the expressed locus as carrying the imprinting signal. *Cell*. 1993;73(1):61–71.
- [34] Jiang X, Liu C, Yu T, et al. Genetic dissection of the down syndrome critical region. *Hum Mol Genet*. 2015;24(22):6540–6551.



- [35] Antonaros F, Pitocco M, Abete D, et al. Structural characterization of the highly restricted down syndrome critical region on 21q22.13: new *KCNJ6* and *DSCR4* transcript isoforms. *Front Genet.* **2021**;12:770359.
- [36] Alves da Silva AF, Machado FB, Pavarino EC, et al. Trisomy 21 alters DNA methylation in parent-of-origin-dependent and -independent manners. *PLoS One.* **2016**;11(4):e0154108.
- [37] Shaaban S, MacKinnon S, Andrews C, et al. Genome-wide association study identifies a susceptibility locus for comitant Esotropia and suggests a parent-of-origin effect. *Invest Ophthalmol Vis Sci.* **2018**;59(10):4054–4064.
- [38] Das Chakraborty R, Bernal AJ, Schoch K, et al. Dysregulation of *DGCR6* and *DGCR6L*: psychopathological outcomes in chromosome 22q11.2 deletion syndrome. *Transl Psychiatry.* **2012**;2:e105.
- [39] Motahari Z, Moody SA, Maynard TM, et al. In the line-up: deleted genes associated with DiGeorge/22q11.2 deletion syndrome: are they all suspects? *J Neurodev Disord.* **2019**;11(1):7.
- [40] Catusi I, Garzo M, Capra AP, et al. 8p23.2-pter microdeletions: seven new cases narrowing the candidate region and review of the literature. *Genes (Basel).* **2021**;12(5):652.
- [41] Seale P, Bjork B, Yang W, et al. *PRDM16* controls a brown fat/skeletal muscle switch. *Nature.* **2008**;454(7207):961–967.
- [42] Luedi PP, Hartemink AJ, Jirtle RL. Genome-wide prediction of imprinted murine genes. *Genome Res.* **2005**;15(6):875–884.
- [43] Wylie AA, Murphy SK, Orton TC, et al. Novel imprinted *DLK1/GTL2* domain on human chromosome 14 contains motifs that mimic those implicated in *IGF2/H19* regulation. *Genome Res.* **2000**;10(11):1711–1718.
- [44] Davies W, Isles A, Smith R, et al. *Xlr3b* is a new imprinted candidate for X-linked parent-of-origin effects on cognitive function in mice. *Nat Genet.* **2005**;37(6):625–629.
- [45] Zhang G, Luo Y, Li G, et al. *DHRXS*, a novel non-classical secretory protein associated with starvation induced autophagy. *Int J Med Sci.* **2014**;11(9):962–970.
- [46] Skuse DH, James RS, Bishop DV, et al. Evidence from Turner's syndrome of an imprinted X-linked locus affecting cognitive function. *Nature.* **1997**;387(6634):705–708.
- [47] Bailey TL, Johnson J, Grant CE, et al. The MEME suite. *Nucleic Acids Res.* **2015**;43(W1):W39–49.
- [48] Bartolomei MS, Tilghman SM. Genomic imprinting in mammals. *Annu Rev Genet.* **1997**;31:493–525.
- [49] Murphy SK, Jirtle RL. Imprinting evolution and the price of silence. *Bioessays.* **2003**;25(6):577–588.
- [50] Jassal B, Matthews L, Viteri G, et al. The reactome pathway knowledgebase. *Nucleic Acids Res.* **2020**;48(D1):D498–D503.
- [51] Davis AP, Grondin CJ, Johnson RJ, et al. The comparative toxicogenomics database: update 2019. *Nucleic Acids Res.* **2019**;47(D1):D948–D954.
- [52] Gunasekara CJ, Scott CA, Laritsky E, et al. A genomic atlas of systemic interindividual epigenetic variation in humans. *Genome Biol.* **2019**;20(1):105.
- [53] Dell'Aversana C, Cuomo F, Longobardi S, et al. Age-related miRNome landscape of cumulus oophorus cells during controlled ovarian stimulation protocols in IVF cycles. *Hum Reprod.* **2021**;36(5):1310–1325.
- [54] Poduval DB, Ognedal E, Sichmanova Z, et al. Assessment of tumor suppressor promoter methylation in healthy individuals. *Clin Epigenetics.* **2020**;12(1):131.
- [55] Becerril S, Gomez-Ambrosi J, Martin M, et al. Role of *PRDM16* in the activation of brown fat programming. Relevance to the development of obesity. *Histol Histopathol.* **2013**;28(11):1411–1425.
- [56] Hoyo C, Murtha AP, Schildkraut JM, et al. Folic acid supplementation before and during pregnancy in the Newborn Epigenetics Study (NEST). *BMC Public Health.* **2011**;11(1):46.
- [57] King K, Murphy S, Hoyo C. Epigenetic regulation of Newborns' imprinted genes related to gestational growth: patterning by parental race/ethnicity and maternal socioeconomic status. *J Epidemiol Community Health.* **2015**;69(7):639–647.
- [58] Vidal AC, Benjamin Neelon SE, Liu Y, et al. Maternal stress, preterm birth, and DNA methylation at imprint regulatory sequences in humans. *Genet Epigenet.* **2014**;6:37–44.
- [59] Cui H, Cruz-Correa M, Giardiello FM, et al. Loss of *IGF2* imprinting: a potential marker of colorectal cancer risk. *Science.* **2003**;299(5613):1753–1755.
- [60] Nakagawa H, Chadwick RB, Peltomaki P, et al. Loss of imprinting of the insulin-like growth factor II gene occurs by biallelic methylation in a core region of *H19*-associated CTCF-binding sites in colorectal cancer. *Proc Natl Acad Sci U S A.* **2001**;98(2):591–596.
- [61] Sullivan MJ, Taniguchi T, Jhee A, et al. Relaxation of *IGF2* imprinting in Wilms tumours associated with specific changes in *IGF2* methylation. *Oncogene.* **1999**;18(52):7527–7534.
- [62] Ulaner GA, Vu TH, Li T, et al. Loss of imprinting of *IGF2* and *H19* in osteosarcoma is accompanied by reciprocal methylation changes of a CTCF-binding site. *Hum Mol Genet.* **2003**;12(5):535–549.
- [63] Horvath S, Raj K. DNA methylation-based biomarkers and the epigenetic clock theory of ageing. *Nat Rev Genet.* **2018**;19(6):371–384.
- [64] Levine ME, Lu AT, Quach A, et al. An epigenetic biomarker of aging for lifespan and healthspan. *Aging (Albany NY).* **2018**;10(4):573–591.
- [65] Ray S, McEvoy DS, Aaron S, et al. Using statistical anomaly detection models to find clinical decision support malfunctions. *J Am Med Inform Assoc.* **2018**;25(7):862–871.
- [66] Roberts E, Zhao L. A Bayesian mixture model for changepoint estimation using ordinal predictors. *Int J Biostat.* **2021**;18:57–72.